Ultrafast equilibration of excited electrons in dynamical simulations

2009 J. Phys.: Condens. Matter 21 485503

(http://iopscience.iop.org/0953-8984/21/48/485503)

IOP PUBLISHING JOURNAL OF PHYSICS: CONDENSED MATTER

J. Phys.: Condens. Matter **21** (2009) 485503 (6pp) doi:10.1088/0953-8984/21/48/485503

Ultrafast equilibration of excited electrons in dynamical simulations

Zhibin Lin[1] **and Roland E Allen**

Department of Physics, Texas A&M University, College Station, TX 77843, USA

E-mail: allen@tamu.edu

Received 30 July 2009, in final form 18 October 2009
Published 6 November 2009
Online at stacks.iop.org/JPhysCM/21/485503

Abstract

In our density-functional-based simulations of materials responding to femtosecond-scale laser pulses, we have observed a potentially useful phenomenon: the excited electrons automatically equilibrate to a Fermi–Dirac distribution within ∼100 fs, solely because of their coupling to the nuclear motion, even though the resulting electronic temperature is one to two orders of magnitude higher than the kinetic temperature defined by the nuclear motion. Microscopic simulations like these can then provide the separate electronic and kinetic temperatures, chemical potentials, pressures, and nonhydrostatic stresses as input for studies on larger lengths and timescales.

(Some figures in this article are in colour only in the electronic version)

1. Motivation

It has been experimentally observed in metals [1–7], semiconductors [8–11], and other materials, including graphite [12–14], that electrons tend to equilibrate first with each other (within a few hundred femtoseconds or less) and then with the motion of the nuclei (within a few picoseconds or less) after the application of a femtosecond-scale laser pulse. Immediately following application of the pulse, therefore, the material is typically characterized by separate electronic and kinetic (or 'lattice') temperatures [15–19]. There are, of course, subtleties involving, for example, interaction of electron and hole subsystems [20].

None of these equilibration processes can occur in a simulation of the electron dynamics which is based on a mean-field description such as time-dependent density-functional theory [21, 22], if there is also no motion of the nuclei. The mechanisms normally invoked for femtosecond-scale equilibration of the electronic subsystem involve electron correlations of one kind or another, which are omitted in a mean-field treatment.

Here we find that there is a second mechanism for femtosecond-scale equilibration of the electronic subsystem: coupling of the electrons to the nuclear motion. This means that electronic equilibration can occur even in mean-field simulations, including density-functional or density-functional-based simulations, as long as the motion of the nuclei is included. The *timescale*, and the interesting *complications and nuances* of electronic equilibration (exemplified by observations like those of [14]) are certainly not well described in a simulation which includes only this mechanism. Nevertheless, if the coupling of the electrons to the electromagnetic field (or other exciting perturbation) is correct, the initial value of the electron temperature and chemical potential should also be reliable for those cases where the electronic energy is approximately conserved during equilibration (and where subtleties such as separate electron and hole temperatures are not important), since any mechanism or combination of mechanisms that leads to a Fermi–Dirac distribution at fixed total energy and number of particles will yield the same temperature and chemical potential.

The result found below is thus potentially useful in various contexts. For example, it means that microscopic quantum simulations with a technique like the present one, or those reviewed in [21] and [22], can provide an electronic temperature T_e, an electronic chemical potential μ_e, and a kinetic temperature T_n (associated with nuclear motion) as input into more macroscopic simulations on larger lengths and timescales, in a multi-scale scheme which employs classical descriptions such as a two-temperature model [15–19]. As shown below, the present method can similarly provide the

[1] Present address: Renewable Energy Materials Research Science and Engineering Center (REMRSEC), Department of Physics, Colorado School of Mines, Golden, CO 80401, USA.

separate electronic and kinetic contributions to the pressure and nonhydrostatic stresses for larger-scale calculations in such a hierarchical scheme, via equations (16) and (17).

2. Method

We call our method semiclassical electron-radiation–ion dynamics (SERID) to emphasize its central features and its central approximation, which is a classical treatment of both the radiation field and the nuclear motion. The electrons are treated in a time-dependent density-functional-based picture, and are represented by nonorthogonal basis functions which move with the nuclei, so that the time-dependent Schrödinger equation has the form [23, 24]

$$\mathrm{i}\hbar\frac{\partial}{\partial t}\boldsymbol{\psi}_n(t) = \boldsymbol{S}^{-1}\cdot\boldsymbol{H}\cdot\boldsymbol{\psi}_n(t) \tag{1}$$

where $\boldsymbol{S}$ is the overlap matrix. The nuclear motion is described by the Ehrenfest equation [23, 24]

$$M\frac{\mathrm{d}^2X}{\mathrm{d}t^2} = -\frac{1}{2}\sum_n \boldsymbol{\psi}_n^\dagger\cdot\left(\frac{\partial\boldsymbol{H}}{\partial X} - \mathrm{i}\hbar\frac{\partial\boldsymbol{S}}{\partial X}\frac{\partial}{\partial t}\right)\cdot\boldsymbol{\psi}_n + \mathrm{h.c.} - \frac{\partial\mathcal{U}_{\mathrm{rep}}}{\partial X} \tag{2}$$

where X is any nuclear coordinate, M is the corresponding mass, and 'h.c.' means 'Hermitian conjugate'. The density-functional-based Hamiltonian $\boldsymbol{H}$, overlap matrix $\boldsymbol{S}$, and effective ion–ion interaction U_{rep} are determined by the results and methodology of Frauenheim and co-workers [26, 27], which have proved successful in a wide variety of contexts. Finally, the electrons are coupled to the radiation field through the time-dependent Peierls substitution [24, 25].

$$H(\ell',\ell) = H_0(\ell',\ell)\mathrm{e}^{\mathrm{i}q\boldsymbol{A}(t)\cdot(\boldsymbol{X}'-\boldsymbol{X})/\hbar c} \tag{3}$$

where $\boldsymbol{A}(t)$ is the vector potential and $q=-e$. Further details of our general method are given elsewhere [28, 29].

We model any material by a supercell, with periodic boundary conditions on the nuclear motion and electronic density. The basis functions ('atomic orbitals') in a given cell are labeled by the position $\boldsymbol{R}$ of the cell plus an index $\bar{\ell}$ which specifies a nucleus within the cell and an orbital centered on that nucleus: $\ell \leftrightarrow \bar{\ell}, \boldsymbol{R}$. The one-electron states are taken to have the Bloch form

$$\boldsymbol{\psi}_n(\ell) = u_s(\bar{\ell};\boldsymbol{k})\mathrm{e}^{\mathrm{i}\boldsymbol{k}\cdot\boldsymbol{R}}, \qquad n\leftrightarrow\boldsymbol{k},s. \tag{4}$$

Substitution into (1) and (2) gives

$$\mathrm{i}\hbar\sum_{\bar{\ell}'}\bar{S}(\bar{\ell};\bar{\ell}';\boldsymbol{k})\frac{\partial}{\partial t}u_s(\bar{\ell}';\boldsymbol{k}) = \sum_{\bar{\ell}'}\bar{H}(\bar{\ell};\bar{\ell}';\boldsymbol{k})u_s(\bar{\ell}';\boldsymbol{k})$$

or

$$\mathrm{i}\hbar\frac{\partial}{\partial t}\boldsymbol{u}_s(\boldsymbol{k}) = \overline{\boldsymbol{S}}(\boldsymbol{k})^{-1}\cdot\bar{\boldsymbol{H}}(\boldsymbol{k})\cdot\boldsymbol{u}_s(\boldsymbol{k}) \tag{5}$$

and

$$M\frac{\mathrm{d}^2X}{\mathrm{d}t^2} = -\frac{1}{2}\sum_{\boldsymbol{k},s}\boldsymbol{u}_s^\dagger(\boldsymbol{k})\cdot\left(\frac{\partial\bar{\boldsymbol{H}}(\boldsymbol{k})}{\partial X} - \mathrm{i}\hbar\frac{\partial\overline{\boldsymbol{S}}(\boldsymbol{k})}{\partial X}\frac{\partial}{\partial t}\right)\cdot\boldsymbol{u}_s(\boldsymbol{k}) + \mathrm{h.c.} - \frac{\partial U_{\mathrm{rep}}}{\partial X} \tag{6}$$

where the coordinate X is in the cell labeled by $\boldsymbol{R}$, U_{rep} involves only the interactions of the nuclei in this cell with their neighbors, and

$$\bar{S}(\bar{\ell};\bar{\ell}';\boldsymbol{k}) = \sum_{\boldsymbol{R}'-\boldsymbol{R}} S(\bar{\ell},\bar{\ell}';\boldsymbol{R}'-\boldsymbol{R})\mathrm{e}^{\mathrm{i}\boldsymbol{k}\cdot(\boldsymbol{R}'-\boldsymbol{R})} \tag{7}$$

$$\bar{H}(\bar{\ell};\bar{\ell}';\boldsymbol{k}) = \sum_{\boldsymbol{R}'-\boldsymbol{R}} H(\bar{\ell},\bar{\ell}';\boldsymbol{R}'-\boldsymbol{R})\mathrm{e}^{\mathrm{i}\boldsymbol{k}\cdot(\boldsymbol{R}'-\boldsymbol{R})}. \tag{8}$$

As mentioned above, simulations with the present approach can also yield the 'electronic stress tensor' $\sigma^{\mathrm{e}}_{\alpha\beta}$, which can be defined by [30, 31].

$$\sigma^{\mathrm{e}}_{\alpha\beta} = -\frac{1}{\mathcal{V}}\frac{\partial\mathcal{E}_{\mathrm{e}}}{\partial\eta_{\alpha\beta}} \tag{9}$$

where $\mathcal{V}$ is the volume of the system, $\eta_{\alpha\beta}$ is the strain, α and β are coordinate labels, and

$$\mathcal{E}_{\mathrm{e}} = \sum_n \boldsymbol{\psi}_n^\dagger\cdot\boldsymbol{H}\cdot\boldsymbol{\psi}_n + \mathcal{U}_{\mathrm{rep}} \tag{10}$$

is the 'electronic energy', with the total energy equal to $\mathcal{E}_{\mathrm{e}}$ plus the kinetic energy of the nuclei (or, more precisely, of the ion cores). Write $\boldsymbol{\psi}_n$ in terms of the instantaneous one-electron eigenstates $\bar{\boldsymbol{\psi}}_j$:

$$\boldsymbol{\psi}_n = \sum_j c_{n,j}\,\bar{\boldsymbol{\psi}}_j \tag{11}$$

$$\boldsymbol{H}\cdot\bar{\boldsymbol{\psi}}_j = \varepsilon_j\,\boldsymbol{S}\cdot\bar{\boldsymbol{\psi}}_j, \qquad \bar{\boldsymbol{\psi}}_i^\dagger\cdot\boldsymbol{S}\cdot\bar{\boldsymbol{\psi}}_j = N\delta_{ij} \tag{12}$$

where N is the number of cells. We then have

$$\mathcal{E} = N\sum_j n_j\varepsilon_j + \mathcal{U}_{\mathrm{rep}} \tag{13}$$

where

$$n_j = \sum_n |c_{n,j}|^2,\ c_{n,j} = \bar{\boldsymbol{\psi}}_j^\dagger\cdot\boldsymbol{S}\cdot\boldsymbol{\psi}_n/N \tag{14}$$

or

$$n_s(\boldsymbol{k}) = \sum_{k,s'}|c_{s',s}(\boldsymbol{k})|^2, \qquad c_{s',s}(\boldsymbol{k}) = \bar{\boldsymbol{u}}_s^\dagger(\boldsymbol{k})\cdot\boldsymbol{S}\cdot\boldsymbol{u}_{s'}(\boldsymbol{k}) \tag{15}$$

where $\bar{\boldsymbol{\psi}}_j(\ell) = \bar{u}_s(\bar{\ell};\boldsymbol{k})\exp(\mathrm{i}\boldsymbol{k}\cdot\boldsymbol{R})$. The fact that

$$\bar{\boldsymbol{\psi}}_j^\dagger\cdot\boldsymbol{S}\cdot\boldsymbol{\psi}_n = \sum_{\bar{\ell},\boldsymbol{R};\bar{\ell}'}\bar{u}_s^\dagger(\bar{\ell};\boldsymbol{k})\mathrm{e}^{\mathrm{i}(\boldsymbol{k}'-\boldsymbol{k})\cdot\boldsymbol{R}}S(\bar{\ell},\bar{\ell}';\boldsymbol{k}')u_{s'}(\bar{\ell}';\boldsymbol{k}') = N\sum_{\bar{\ell},\bar{\ell}'}\bar{u}_s^\dagger(\bar{\ell};\boldsymbol{k}')S(\bar{\ell},\bar{\ell}';\boldsymbol{k}')u_{s'}(\bar{\ell}';\boldsymbol{k}')$$

has been used. (In the last step, $\boldsymbol{k}'-\boldsymbol{k}$ cannot be equal to a nonzero reciprocal lattice vector because $\boldsymbol{k}$ and $\boldsymbol{k}'$ are restricted to the first Brillouin zone.) But since

$$\frac{\partial\varepsilon_j}{\partial\eta_{\alpha\beta}} = \frac{\partial\bar{\boldsymbol{\psi}}_j^\dagger}{\partial\eta_{\alpha\beta}}\cdot\boldsymbol{H}\cdot\bar{\boldsymbol{\psi}}_j + \bar{\boldsymbol{\psi}}_j^\dagger\cdot\frac{\partial\boldsymbol{H}}{\partial\eta_{\alpha\beta}}\cdot\bar{\boldsymbol{\psi}}_j + \bar{\boldsymbol{\psi}}_j^\dagger\cdot\boldsymbol{H}\cdot\frac{\partial\bar{\boldsymbol{\psi}}_j}{\partial\eta_{\alpha\beta}}$$
$$= \varepsilon_j\frac{\partial}{\partial\eta_{\alpha\beta}}(\bar{\boldsymbol{\psi}}_j^\dagger\cdot\boldsymbol{S}\cdot\bar{\boldsymbol{\psi}}_j) - \varepsilon_j\left(\bar{\boldsymbol{\psi}}_j^\dagger\cdot\frac{\partial\boldsymbol{S}}{\partial\eta_{\alpha\beta}}\cdot\bar{\boldsymbol{\psi}}_j\right)$$
$$+ \bar{\boldsymbol{\psi}}_j^\dagger\cdot\frac{\partial\boldsymbol{H}}{\partial\eta_{\alpha\beta}}\cdot\bar{\boldsymbol{\psi}}_j = \bar{\boldsymbol{\psi}}_j^\dagger\cdot\left(\frac{\partial\boldsymbol{H}}{\partial\eta_{\alpha\beta}} - \frac{\partial\boldsymbol{S}}{\partial\eta_{\alpha\beta}}\varepsilon_j\right)\cdot\bar{\boldsymbol{\psi}}_j$$

it follows that

$$\sigma^{\mathrm{e}}_{\alpha\beta} = -\frac{1}{\mathcal{V}}\left[\sum_j n_j \bar{\boldsymbol{\psi}}^{\dagger}_j \cdot \left(\frac{\partial \boldsymbol{H}}{\partial \eta_{\alpha\beta}} - \frac{\partial \boldsymbol{S}}{\partial \eta_{\alpha\beta}}\varepsilon_j\right)\cdot \bar{\boldsymbol{\psi}}_j + \frac{\partial \mathcal{U}_{\mathrm{rep}}}{\partial \eta_{\alpha\beta}}\right]$$
$$= -\frac{1}{V}\left[\sum_{\boldsymbol{k},s} n_s(\boldsymbol{k})\bar{\boldsymbol{u}}^{\dagger}_s(\boldsymbol{k}) \cdot \left(\frac{\partial \bar{\boldsymbol{H}}(\boldsymbol{k})}{\partial \eta_{\alpha\beta}} - \frac{\partial \bar{\boldsymbol{S}}(\boldsymbol{k})}{\partial \eta_{\alpha\beta}}\varepsilon_j\right)\cdot \bar{\boldsymbol{u}}_s(\boldsymbol{k}) + \frac{\partial U_{\mathrm{rep}}}{\partial \eta_{\alpha\beta}}\right] \quad (16)$$

where V is the volume of one cell. This has the same form as equation (6), but the derivation and physical content are different.

The above derivation is valid for any parameter λ that changes the Hamiltonian and overlap matrices, with $\eta_{\alpha\beta} \to \lambda$ and $-\mathcal{V}\sigma^{\mathrm{e}}_{\alpha\beta} \to \partial\mathcal{E}_{\mathrm{e}}/\partial\lambda$ in (9), so the 'electronic pressure' is given by

$$P_{\mathrm{e}} = -\left[\sum_j n_j \bar{\boldsymbol{\psi}}^{\dagger}_j \cdot \left(\frac{\partial \boldsymbol{H}}{\partial \mathcal{V}} - \frac{\partial \boldsymbol{S}}{\partial \mathcal{V}}\varepsilon_j\right)\cdot \bar{\boldsymbol{\psi}}_j + \frac{\partial \mathcal{U}_{\mathrm{rep}}}{\partial \mathcal{V}}\right]$$
$$= -\left[\sum_{\boldsymbol{k},s} n_s(\boldsymbol{k})\bar{\boldsymbol{u}}^{\dagger}_s(\boldsymbol{k}) \cdot \left(\frac{\partial \bar{\boldsymbol{H}}(\boldsymbol{k})}{\partial V} - \frac{\partial \bar{\boldsymbol{S}}(\boldsymbol{k})}{\partial V}\varepsilon_j\right)\cdot \bar{\boldsymbol{u}}_s(\boldsymbol{k}) + \frac{\partial U_{\mathrm{rep}}}{\partial V}\right]. \quad (17)$$

It is straightforward to calculate the additional kinetic contributions to the pressure and nonhydrostatic stresses using standard molecular-dynamics methods [32, 33].

3. Results

The simulations reported here are for a double layer of graphene, with each layer containing 112 carbon atoms. Periodic boundary conditions are imposed in the lateral directions, so the equations developed in the preceding section are appropriate, with $\boldsymbol{k}$ and $\boldsymbol{R}$ two-dimensional vectors. However, since the system is relatively large (with 896 orbitals), we take the electronic states as well as the nuclear positions to be periodic; i.e., we take $\boldsymbol{k} = 0$. In the simulations reported below, the laser pulse had a duration of 45 femtoseconds (FWHM), an effective photon energy of 1.55 eV, and a fluence of 3.0 kJ m^{-2}, with the polarization vector inclined at 45° with respect to the surface normal. A time step of 50 attoseconds was used in numerically solving both the time-dependent Schrödinger equation and the nuclear equations of motion. Figure 1 shows the occupancy of equation (15)

$$n_s = \sum_{s'} |c_{s',s}|^2, \qquad c_{s',s} = \bar{\boldsymbol{u}}^{\dagger}_s \cdot \boldsymbol{S} \cdot \boldsymbol{u}_{s'} \quad (18)$$

for each electronic eigenstate labeled by s as a function of the energy eigenvalue ε_s, at 10 and 55 fs, with the full duration of the laser pulse extending from 10 to 100 fs.

Recall that the actual one-electron states are determined by the time-dependent Schrödinger equation, equation (5),

$$\mathrm{i}\hbar\frac{\partial}{\partial t}\boldsymbol{u}_s = \bar{\boldsymbol{S}}^{-1} \cdot \bar{\boldsymbol{H}} \cdot \boldsymbol{u}_s \quad (19)$$

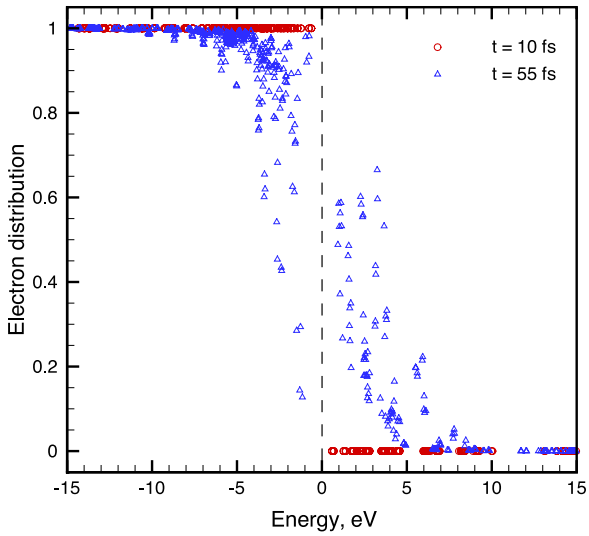

Figure 1. Electron distribution $n_{\mathrm{e}}(\varepsilon)$ for a double layer of graphene subjected to a laser pulse with a 45 fs duration (FWHM) and an effective photon energy of 1.55 eV. The pulse starts at 10 fs and ends at 100 fs. Prior to the pulse, all states below the Fermi energy are occupied, and all states above are unoccupied. At 55 fs, electronic excitation has resulted in a distribution that is far out of equilibrium.

whereas the eigenstates are the solutions to

$$\bar{\boldsymbol{H}} \cdot \bar{\boldsymbol{u}}_s = \varepsilon_s \bar{\boldsymbol{S}} \cdot \bar{\boldsymbol{u}}_s. \quad (20)$$

Figure 1 thus shows $n_{\mathrm{e}}(\varepsilon)$, the occupancy of an eigenstate at a given time as a function of its energy. For a fully equilibrated Fermi–Dirac distribution at temperature T_{e} we would have

$$n_{\mathrm{e}}(\varepsilon) = \frac{1}{1 + \mathrm{e}^{(\varepsilon-\mu_{\mathrm{e}})/kT_{\mathrm{e}}}}. \quad (21)$$

Although the system is initially equilibrated at a temperature of 300 K, the initial electron distribution of figure 1, at $t = 10$ fs, is essentially indistinguishable from a step function. After one-half the full pulse duration, electrons have been strongly excited over a range of several eV near the Fermi surface, and the distribution is very far from equilibrium. However, figure 2 shows that at the end of the pulse, $t = 100$ fs, there is already a tendency for the electrons to form up into a Fermi–Dirac distribution, via transitions between the energy levels.

Figure 3 shows that the distribution $n_{\mathrm{e}}(\varepsilon)$ at $t = 200$ fs is very close to a proper Fermi–Dirac distribution. A fit of equation (21) to the data, also shown in figure 3, yields an electron temperature of 20 880 K (corresponding to 1.8 eV) and a chemical potential of 0.75 eV relative to the initial Fermi energy.

On the other hand, the average 'lattice' temperature T_{n}, calculated from the kinetic energy of the nuclei, is found to be 860 K at 200 fs. This very substantial increase in the nuclear kinetic energy results from modification of the interatomic (Hellmann–Feynman) forces when the laser pulse promotes large numbers of electrons to excited states. It is interesting to observe the effect of T_{n} on the pair correlation function, which is increasingly broadened by the thermal motion of the nuclei

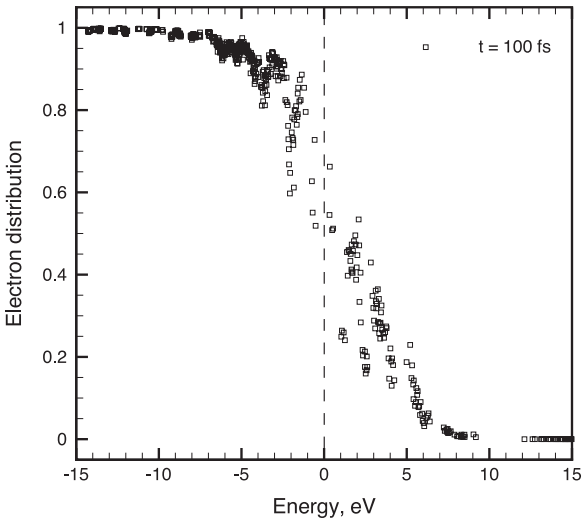

Figure 2. Electron distribution at 100 fs, exhibiting an approach to equilibrium on this timescale.

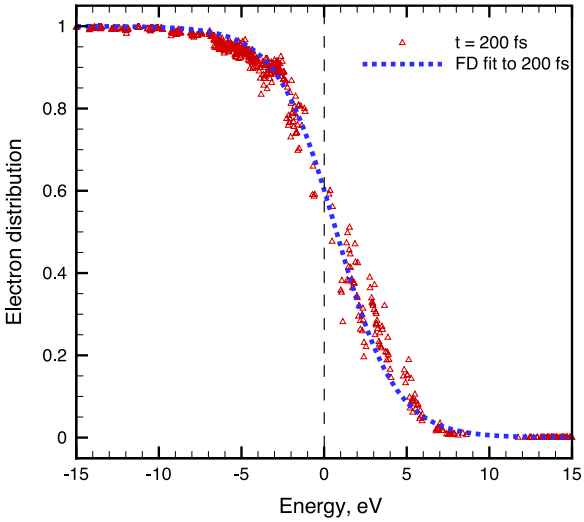

Figure 3. Electron distribution at 200 fs. The dashed line is a fit to a Fermi–Dirac distribution with an electron temperature of 20 880 K and a chemical potential of 0.75 eV.

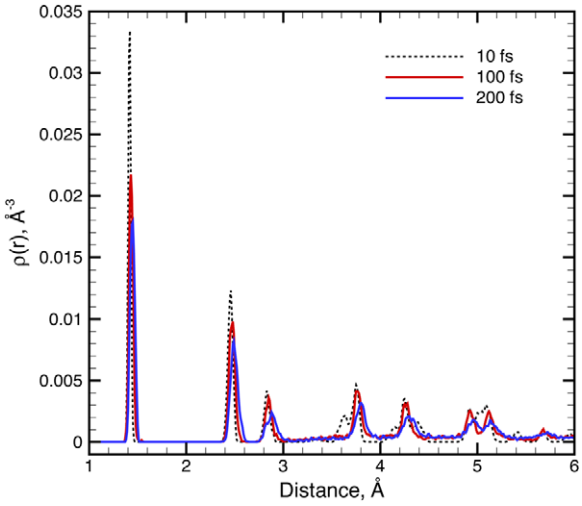

Figure 4. Pair correlation function at 10, 100, and 200 fs, with a broadening that increases with time as the thermal motion of the nuclei increases.

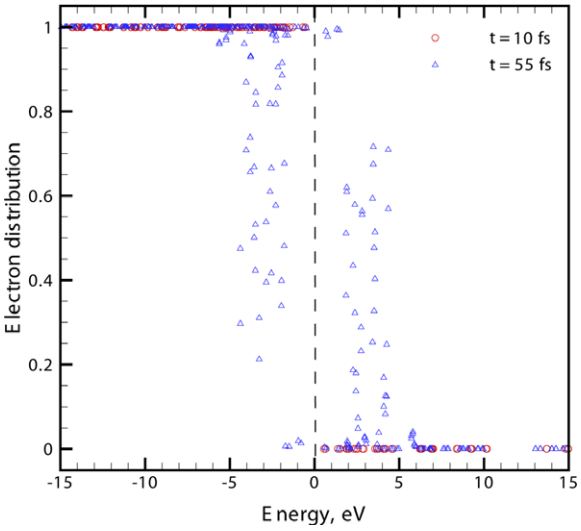

Figure 5. Electron distribution for the same laser pulse as in figure 1 but with the nuclei not allowed to move. The pulse again starts at 10 fs and finishes at 100 fs. At 55 fs, there is no tendency toward electronic equilibration.

with increasing time, as can be seen in figure 4. However, T_n is still one or two orders of magnitude less than T_e.

To see whether this remarkable outcome is in fact due to the nuclear motion, we repeated the simulation with exactly the same laser pulse, but with the nuclei frozen in place. In figure 5 the electrons are again excited from initially occupied states below the Fermi energy to initially unoccupied states above, but there is no tendency toward equilibration.

In figure 6, which should be compared with figures 2 and 3, there is no tendency whatsoever for the electrons to equilibrate, and there cannot be, of course, because there is no perturbation from either a radiation field or nuclear motion to induce electronic transitions after completion of the pulse. In fact, many of the states in figure 6 never exhibit any transitions at all, because there are selection rules which apply with the perfect symmetry of the ground-state geometry, but which are broken when this symmetry is broken by the complex nuclear motion in the more physical simulation of figures 1–3.

The above results indicate that ion motion causes the excited electrons to equilibrate within ∼100 fs. In order to investigate how the electron equilibration time changes with respect to the degree of laser excitation, we performed simulations for two lower fluences, 1.0 and 1.3 kJ m^{-2}, while keeping the other properties of the laser pulse unchanged. Just as in the case of the substantially higher fluence above (3.0 kJ m^{-2}), electrons were again found to rapidly equilibrate as a result of ion motion. In figure 7, the electron distribution is shown at 55 and 150 fs after application of a pulse with a fluence of 1.3 kJ m^{-2}. By fitting the electron distribution at 150 fs to the Fermi–Dirac function, one obtains an effective electron temperature of 13 920 K (corresponding to 1.2 eV),

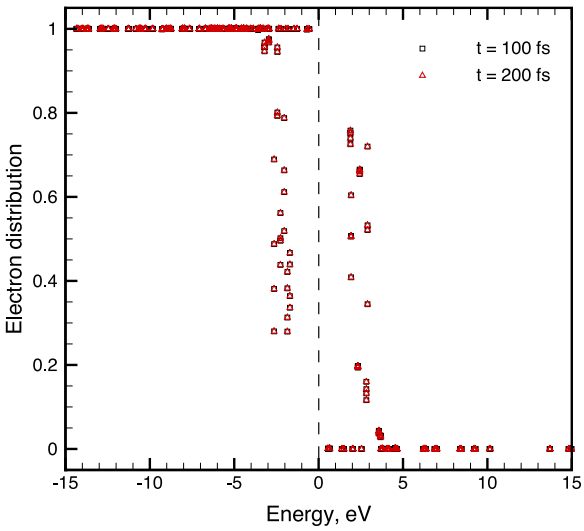

Figure 6. Electron distributions at 100 and 200 fs, with the nuclei not allowed to move. Notice that the electron distributions at these two times are completely identical. I.e., there are no electronic transitions because there are no perturbations from either the radiation field or nuclear motion. Compare with figures 2 and 3.

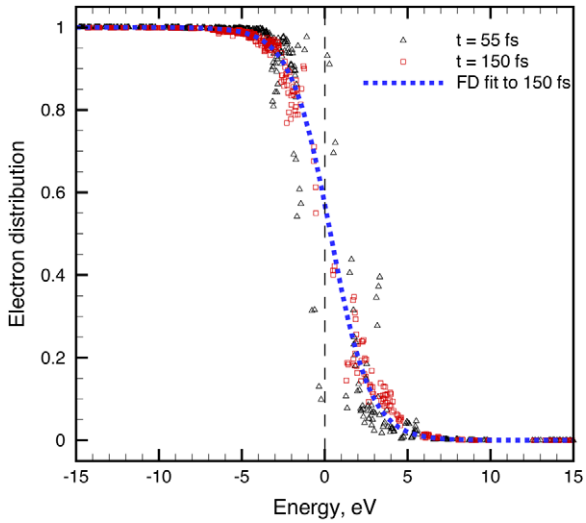

Figure 7. Electron distribution at 55 and 150 fs for a laser fluence of 1.3 kJ m^{-2}. The dashed line is a fit to a Fermi–Dirac distribution with an electron temperature of 13 920 K and a chemical potential of 0.35 eV.

and a chemical potential of 0.35 eV relative to the initial Fermi energy.

Note that the electron temperatures for the two fluences, given by the Fermi–Dirac fits of figures 3 and 7 respectively, are consistent with the amount of laser energy absorbed by the material. On the other hand, the equilibration time is shorter, about 50 fs, for the lower fluence. A still lower equilibration time, less than 50 fs, was found for the still lower fluence of 1.0 kJ m^{-2}. This decrease in equilibration time appears to be related to the fact that electrons are excited to energies less far away from the Fermi level at the lower fluences, while the sizable ion motion is still effective in causing the excited electrons to equilibrate. It should be mentioned that careful examination of figure 6 shows that the occupancy at some energy levels does not exactly correspond to a Fermi distribution, and precise convergence to this distribution may require a considerably longer time than the approximate equilibration observed here. Nevertheless, the average relaxation times for the lower fluences are found to be smaller than that at high fluence.

4. Conclusion

The above results demonstrate that equilibration of the electronic subsystem on a femtosecond timescale results from the coupling of electrons to nuclear motion, even when electron correlations are completely omitted. The significance and potential utility of this result are discussed in the first section, so here we simply offer a qualitative explanation: the electrons are coupled to the nuclear motion through equations (1) and (2): the nuclear positions determine the electronic Hamiltonian, so perturbations in the nuclear positions induce electronic transitions, just as in our previous studies of molecular processes [34], but with much greater frequency in a metal or semimetal because the energy differences are comparable to the effective phonon energies associated with nuclear motion. The nuclei are also influenced by the electrons, whose states determine the interatomic forces of equation (2).

We interpret the relevant aspect of the nuclear motion, in this system with a sizable number of atoms, to be essentially a random jiggling of the electrons that tends to randomize their distribution among the available states—i.e., to maximize their entropy. It is well known that maximization of the entropy in a system of fermions at fixed energy and number of particles leads to a Fermi–Dirac distribution with a well-defined temperature T_e and chemical potential μ_e [35]. In future work, we plan to explore this phenomenon in other materials. For heavier atoms one expects moderately longer equilibration times, but still on a femtosecond scale.

In a comparison of the quasiparticle relaxation rates obtained from time-resolved photoemission experiments and *ab initio* calculations, the timescale was found to range from a few hundreds of femtoseconds to tens of femtoseconds [12]. This appears to imply that the mechanism treated here is comparable in importance to correlation effects, in the specific context of ultrafast electron equilibration.

Acknowledgments

This work was supported by the Robert A. Welch Foundation (Grant A-0929). The authors would like to thank Meng Gao, Chenwei Jiang, and Xiang Zhou for helpful discussions, and the Texas A&M University Supercomputing Facility for the use of its parallel supercomputing resources.

References

[1] Eesley G L 1983 *Phys. Rev. Lett.* **51** 2140
[2] Fujimoto J G, Liu J M, Ippen E P and Bloembergen N 1984 *Phys. Rev. Lett.* **53** 1837

[3] Elsayed-Ali H E, Norris T B, Pessot M A and Mourou G A 1987 *Phys. Rev. Lett.* **58** 1212
[4] Schoenlein R W, Lin W Z, Fujimoto J G and Eesley G L 1987 *Phys. Rev. Lett.* **58** 1680
[5] Brorson S D, Kazeroonian A, Moodera J S, Face D W, Cheng T K, Ippen E P, Dresselhaus M S and Dresselhaus G 1990 *Phys. Rev. Lett.* **64** 2172
[6] Fann W S, Storz R, Tom H W K and Bokor J 1992 *Phys. Rev. Lett.* **68** 2834
[7] Hertel T, Knoesel E, Wolf M and Ertl G 1996 *Phys. Rev. Lett.* **76** 535
[8] Oudar J L, Hulin D, Migus A, Antonetti A and Alexandre F 1985 *Phys. Rev. Lett.* **55** 2074
[9] Knox W H, Hirlimann C, Miller D A B, Shah J, Chemla D S and Shank C V 1986 *Phys. Rev. Lett.* **56** 1191
[10] Elsaesser T, Shah J, Rota L and Lugli P 1991 *Phys. Rev. Lett.* **66** 1757
[11] Goldman J R and Prybyla J A 1994 *Phys. Rev. Lett.* **72** 1364
[12] Moos G, Gahl C, Fasel R, Wolf M and Hertel T 2001 *Phys. Rev. Lett.* **87** 267402
[13] Kampfrath T, Perfetti L, Schapper F, Frischkorn C and Wolf M 2005 *Phys. Rev. Lett.* **95** 187403
[14] Breusing M, Ropers C and Elsaesser T 2009 *Phys. Rev. Lett.* **102** 086809
[15] Kaganov M I, Lifshitz I M and Tanatarov L V 1956 *Zh. Eksp. Teor. Fiz.* **31** 232
Kaganov M I, Lifshitz I M and Tanatarov L V 1957 *Sov. Phys.—JETP* **4** 173 (Engl. Transl.)
[16] Anisimov S I, Kapeliovich B L and Perelman T L 1974 *Zh. Eksp. Teor. Fiz.* **66** 776
Anisimov S I, Kapeliovich B L and Perelman T L 1974 *Sov. Phys.—JETP* **39** 375 (Engl. Transl.)
[17] Allen P B 1987 *Phys. Rev. Lett.* **59** 1460
[18] Ivanov D S and Zhigilei L V 2003 *Phys. Rev.* B **68** 064114
[19] Lin Z, Zhigilei L V and Celli V 2008 *Phys. Rev.* B **77** 075133
[20] Johnson S L, Beaud P, Milne C J, Krasniqi F S, Zijlstra E S, Garcia M E, Kaiser M, Grolimund D, Abela R and Ingold G 2008 *Phys. Rev. Lett.* **100** 155501
[21] Payne M C, Teter M P, Allan D C, Arias T A and Joannopoulos J D 1992 *Rev. Mod. Phys.* **64** 1045
[22] Marques M A L, Ullrich C A, Nogueira F, Rubio A, Burke K and Gross E K U (ed) 2006 *Time-Dependent Density Functional Theory* (Heidelberg: Springer)
[23] Allen R E 1994 *Phys. Rev.* B **50** 18629
[24] Allen R E 2008 *Phys. Rev.* B **78** 064305
[25] Graf M and Vogl P 1995 *Phys. Rev.* B **51** 4940
[26] Porezag D, Frauenheim Th, Köhler Th, Seifert G and Kaschner R 1995 *Phys. Rev.* B **51** 12947
[27] Seifert G, Porezag D and Frauenheim T 1996 *Int. J. Quantum Chem.* **58** 185 See http://www.dftb.org and http://www.dftb-plus.info for the currently best versions
[28] Allen R E, Dumitrica T and Torralva B 2001 *Ultrafast Physical Processes in Semiconductors* ed K T Tsen (New York: Academic)
[29] Dou Y, Torralva B R and Allen R E 2003 *J. Mod. Opt.* **50** 2615
[30] Nielsen O H and Martin R M 1985 *Phys. Rev.* B **32** 3780
[31] Martin R M 2004 *Electronic Structure, Basic Theory and Practical Methods* (Cambridge: Cambridge University Press) p 21 and 59
[32] Parrinello M and Rahman A 1980 *Phys. Rev. Lett.* **45** 1196
[33] Schlick T 2002 *Molecular Modeling and Simulation* (New York: Springer) p 416
[34] See e.g. Jiang C, Xie R, Li F and Allen R E 2009 *Chem. Phys. Lett.* **474** 263
[35] Landau L D and Lifshitz E M 1988 *Statistical Physics* (Oxford: Pergamon) pp 160–1